Indicated Mean Effective Pressure Oscillations in a Natural Gas Combustion Engine

Grzegorz Litak[a,b], Michał Gęca[a,c], Bao-Feng Yao[d], and Guo-Xiu Li[d]

[a] Department of Applied Mechanics, Lublin University of Technology, Nadbystrzycka 36, PL-20-618 Lublin, Poland
[b] Dipartimento di Architettura, Costruzioni e Strutture, Universita Politecnica delle Marche, Via Brecce Bianche, 60131 Ancona, Italy
[c] Department of Thermodynamics, Fluid Mechanics and Aircraft Propulsion, Lublin University of Technology, Nadbystrzycka 36, PL-20-618 Lublin, Poland
[d] School of Mechanical, Electronic and Control Engineering, Beijing Jiaotong University, Beijing 10004, China

Reprint requests to G. L.; E-mail: g.litak@pollub.pl

Z. Naturforsch. **64a,** 393 – 398 (2009); received June 27, 2008 / October 13, 2008

Fluctuations in a combustion process of natural gas in the internal spark ignition engine have been investigated. We measured pressure of the cyclic combustion and expressed its cyclic oscillations in terms of indicated mean effective pressure per cycle. By applying the statistical and multifractal analysis to the corresponding time series we show the considerable changes in engine dynamics for a different equivalence ratio decreases from 0.781 to very lean conditions.

Key words: Engine; Combustion; Nonlinear Oscillations; Multifractals.
PACS numbers: 05.40.C, 05.45.T, 82.40.B

1. Introduction

Nonlinear internal combustion engine dynamics in the contexts of harmful cycle-to-cycle combustion fluctuations has been the subject of intensive research in the last few decades in the context of chaotic and stochastic phenomena [1 – 28]. In the end of eighties of twentieth century Heywood [29] identified three main factors influencing cycle-to-cycle variations: aerodynamic in the cylinder during combustion, the amount of fuel, air and recycled exhaust gases supplied to the cylinder and a mixture composition near the spark plug. Although, the first papers discussed the fluctuations in the combustion of gasoline some recent reports concern fluctuations appearing in natural gas fuel engines [28, 30 – 33]. In most of experimental studies time pressure series were measured inside the combustion chambers. To perform further analysis the series have been estimated in cyclic quantities as the effective pressure (Indicated Mean Effective Pressure – IMEP) [20, 28], the peak pressure $p_{\max}$ [17, 19, 27] or the heat release [4, 8, 14, 15, 18]. In this paper we continue this direction. After estimating the corresponding IMEP time series we perform the statistic and multifractal analysis.

Table 1. Experimental engine specifications.

Cylinder number	6
Bore × Store	126 mm × 130 mm
Displaced volume	9.726 L
Compression ratio	10.5
Intake valve opens	2°BTDC
Intake valve closes	208°ATDC
Exhaust valve opens	227°BTDC
Exhaust valve closes	5°ATDC

2. Experimental Stand and Measurement Procedure

The subject of the present test is a turbocharged 6-cylinder, 4-stroke Diesel engine with an intercooler. The tested unit was adapted for a natural gas engine fed by adding a multi-point port fuel injected system and spark plugs. The total engine cubic capacity is 9.726 dm^3 while the compression ratio is 10.5 : 1. Its geometric details are listed in Table 1. To perform the experiment the engine was mounted on the corresponding test-bed.

The engine torque and power were measured using the 260 kW eddy current dynamometer. The speed of the engine was measured using a 60 tooth sprocket and magnetic pickup. The engine speed and torque

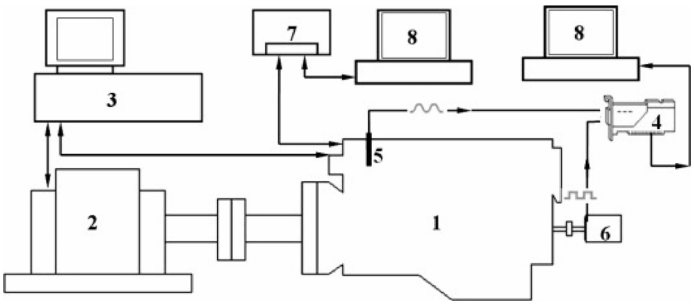

Fig. 1. Scheme of the experimental setup: 1, engine; 2, dynamometer; 3, dynamometer controller; 4, high-speed data acquisition board; 5, pressure transducer; 6, optical encoder; 7, ECU; 8, computer.

were controlled with the special dynamometer controller in conjunction with a throttle controller. Finally the combustion process was monitored using a Kistler 6125B quartz pressure transducer connected to a Kistler 5015A mode charge amplifier. The pressure transducer was located in the head of cylinder No. 6. Though relatively robust to thermal shock, the transducer was mounted through the engine water jacket providing additional cooling and protection from such effects. The crankshaft position was measured using a free end mounted crank shaft encoder that was rigidly mounted to the front of the engine. Its position sensor was connected to the crank shaft with a flexible coupler. Further details on our experimental standing can be found in Li and Yao [28]. Experimental setup see Figure 1.

After measuring pressure in the combustion chamber we have estimated IMEP which is defined as an equivalent constant pressure in a given combustion cycle. This pressure acting on the engine piston during the whole expansion stroke performs the same amount of work as the real variable pressure in the cylinder [29]. It can be expressed as:

$$\mathrm{IMEP} = \mathrm{Li}/\mathrm{Vs}, \tag{1}$$

where Li is the amount work indicated in the cylinder, and Vs is the piston displacement volume. The work Li is estimated numerically by integration of the measured pressure [29].

3. Results and Analysis

The results of our measurements are presented in Figure 2. Note that IMEP(i) was plotted against the cycle number i for the increasing equivalence ratio Φ representing by the lines '1–4'. By numbering 1 to 4 we arranged them in the order of decreasing equivalence ratio from $\Phi = 0.781$ to very lean conditions

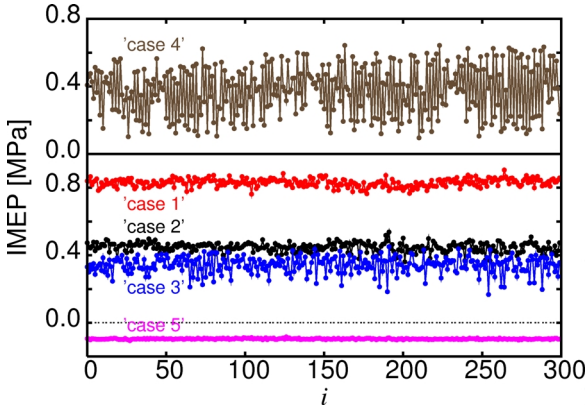

Fig. 2. Cycle-to-cycle changes of IMEP(i), i enumerates the successive cycle. The equivalence ratio $\Phi = 0.781$, 0.677, 0.595, 0.588 for the cases '1–4', respectively. For comparison, the case '5' corresponds to a motored engine.

$\Phi = 0.677$, 0.595, and 0.588, respectively. Interestingly, the IMEP oscillations increase monotonically to reach the maximum in the case '4' (Fig. 2). Simultaneously, the average pressure value $\langle \mathrm{IMEP} \rangle$ is initially decreasing, reaching the minimum at the case '3'. However is growing again in the case '4'. In addition to the lines '1–4' we have also plotted the line '5' corresponding to the pressure time series of a motored engine.

The following is our statistical analysis from calculation of the basic stochastic properties as average values, variances, standard deviations, and higher moments (skewness and kurtosis) using following definitions:

$$\langle X \rangle = \frac{1}{N} \sum_{n=1}^{N} X_n ,$$

$$V_2 = \frac{1}{N-1} \sum_{n=1}^{N} (X_n - \langle X \rangle)^2 , \quad \sigma = \sqrt{V_2} ,$$

$$V_3 = \frac{N}{(N-1)(N-2)} \sum_{n=1}^{N} \left[\frac{X_n - \langle X \rangle}{\sigma} \right]^3 ,$$

Table 2. Definitions of variables and symbols used in the paper.

indicated mean effective pressure	IMEP
average value of IMEP	$\langle \text{IMEP} \rangle$
standard square deviation of IMEP	σ_{IMEP}
variance of IMEP	$V_2(\text{IMEP})$
skewness of IMEP	$V_3(\text{IMEP})$
kurtosis of IMEP	$V_4(\text{IMEP})$
equivalence ratio	$\Phi = 1/\lambda$
cycle number	i
number of considered points in time series	N

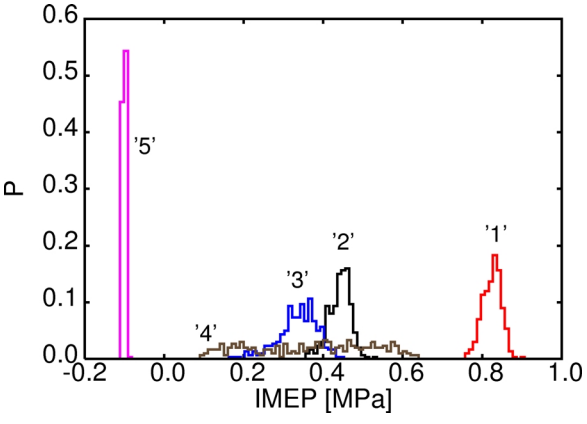

Fig. 3. Distribution of IMEP for the examined cases '1–5' corresponding to Figure 1.

$$V_4 = \frac{N(N+1)}{(N-1)(N-2)(N-3)} \sum_{n=1}^{N} \left[\frac{X_n - \langle X \rangle}{\sigma} \right]^4 - 3\frac{(N-1)^2}{(N-2)(N-3)}, \tag{2}$$

where X_n denotes the consecutive element of the examined time series. Note that definitions of variables and symbols used in the paper are summarized in Table 2.

The distributions of IMEP for examined cases are presented in Figure 3. Note, they differ considerably in their widths and their average values. Starting from the higher equivalence ratio $\Phi = 0.781$ we observe the largest $\langle \text{IMEP} \rangle$ (case '1' in Table 3) and it is decreasing monotonically with decreasing $\Phi =$ to 0.677 and 0.595 (cases '2–3'), respectively. For the smallest $\Phi = 0.376$ one can observe small increase of $\langle \text{IMEP} \rangle$. On the other hand, the standard deviation σ_{IMEP} (Table 3) has the tendency toward increasing to the highest value for the smallest considered Φ. This is an obvious indication of increasing fluctuations. The similar tendency has also been reported in other papers focusing on working on a gasoline fueled engine [26, 27]. In those papers, authors examined the cyclic heat release and the maximum cyclic pressure against the spark ignition advance angle. In some limit of the large advance angle they observed large fluctuation of combustion process including a misfire phenomenon.

Table 3. Summary of statistical and multifractal properties. The engine speed of 1600 r/min was fixed for all cases.

case no.	Φ	$\langle \text{IMEP} \rangle$	σ_{IMEP}	V_3	V_4	Δh	h_0
'1'	0.781	0.829	0.0234	−0.206	−0.020	1.05	0.46
'2'	0.677	0.447	0.0276	−0.452	0.582	1.02	0.59
'3'	0.595	0.342	0.0497	−0.684	0.595	1.49	0.60
'4'	0.588	0.376	0.1502	−0.137	−1.180	1.13	0.67

In our results the effect of noticeable increasing in $\langle \text{IMEP} \rangle$ from the case '3' to the case '4' with decreasing equivalence ratio Φ is also coincided with increasing amplitude of fluctuations measured by a square deviation of IMEP. This can be explained by the appearance of period doubling. Here this phenomenon can be supported by sudden dramatic increase of the mean square deviation with a relatively small change of Φ and the appearance of two maxima in the corresponding histogram (Fig. 3). Evidently, small changes in the mixture composition at spark can produce large changes in combustion because of the highly nonlinear effect of composition and temperature on flame speed [28].

Furthermore the changes in distribution shapes should be commented. In all cases '1–4' one can notice the asymmetry in the probability distribution with the noticeable shift of the most probable values to the right hand side. The change in the flatness of distributions '1–4' is intriguing. With the decreasing equivalence ratio Φ the kurtosis is going from the nearly Gaussian shape '1' to more and more concentrated shape (see cases '2' and '3' in Fig. 3 and Table 3). Finally, in the case '4' one can see the opposite situation. Here the shape is the most flat. Note that the conclusion about the Gaussian shape of IMEP distribution is drawn from the values of kurtosis defined (2) in respect to non-dimensional units (as square deviation). The shapes presented in Fig. 3 are scaled in current values of IMEP and could not be compared directly. More concentrated distributions with $V_4 > 0$ imply the tendency to an intermittent transition of IMEP fluctuations which is evident while changing $\Phi = 0.595$ in the case '3' to 588 in the case '4' [34].

For further study we employed a multifractal algorithm [35] previously used to characterize complex dynamics in other systems. In further studies we propose to use a multifractal analysis [35] which appeared to be a powerful tool to analyze the complexity of the nonlinear systems. This technique has been widely used in

biological systems [36, 37] but recently has been applied in engineering systems, e. g. to examine seismic sequences [38], and to detect cracks in plates [39] or rotors [40]. Recently, it has been also applied to study engine dynamics fueled by gasoline [41]. Following the multifractal procedure [35] we performed the analysis in the small vicinity each cycle i along the examined time series IMEP$(i+\Delta i)$ looking for the exponent h_i (usually non-integer), which estimates the corresponding difference:

$$|\mathrm{IMEP}(i) - \mathrm{IMEP}(i+\Delta i)| \leq a_h \Delta i^{h_i} . \qquad (3)$$

Here a_h is a coefficient related to the exponent h_i determining the local internal separation. The selected examples for the estimation of critical exponents of the 'case 3' time series are presented in Figure 4.

Generally, the multifractal analysis of pressure oscillations is based on constructing a singularity spectrum $f(h)$ of all h_i exponents providing a precise quantitative description of the system behaviour [35–37]. Formally, h defines the Hölder exponent while the probability of its distribution $f(h)$ coincides with the Hausdorff dimension of a dynamical system.

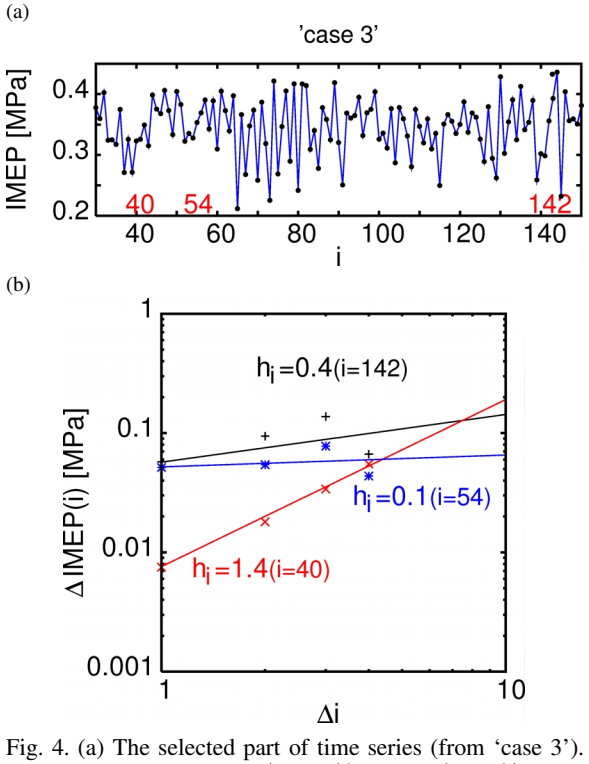

Fig. 4. (a) The selected part of time series (from 'case 3'). (b) Examples of $\Delta\mathrm{IMEP} = |\mathrm{IMEP}(i) - \mathrm{IMEP}(i+\Delta i)|$ versus Δi in the vicinity of $i = 40$, 54 and 142. The slopes in the logarithmic scale are related with corresponding local exponents h_i.

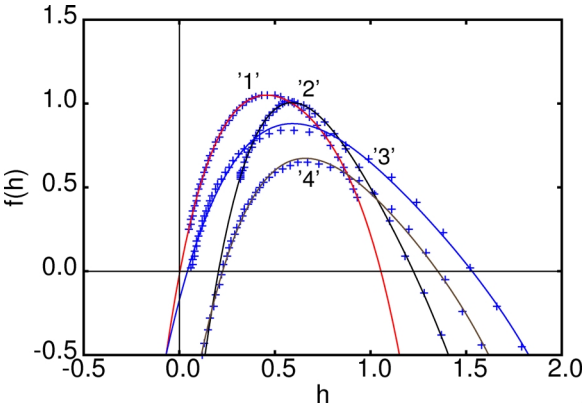

Fig. 5. Distribution of critical exponents $h = h_i$ for examined cases.

The results of our calculations are shown in Figure 5. Note, the width of the spectrum $f(h)$

$$\Delta h = h_{\max} - h_{\min} , \qquad (4)$$

where $h_{\min}$ and $h_{\max}$ are defined to satisfy $f(h) = 0$, is defined as the complexity measure of the system response while the h_0, which corresponds to the maximum of $f(h)$ and represents approximate the average exponent, indicates the randomness of pressure fluctuations.

Note that the value $h_0 = 0.5$ indicate the Brownian motion for which the consecutive steps are fully independent [42]. For $h_0 < 0.5$, the stochastic process is persistent (IMEP of neigbour cycles is correlated positively) while for $h_0 > 0.5$ it is anti-persistent (IMEP of neighbour cycles is correlated negatively). Summarizing the interpretations of Δh and h_0 one can say that the wider the range of possible fractal exponents, the "richer" the dynamical structure, while the larger h_0 means more correlated fluctuations (less random).

Figure 5 and Table 3 show that the system is most complex for the case '3'. Simultaneously, correlations are changing considerably showing that the case '4' is the most correlated. The conclusion is that in this particular case the actual value of IMEP oscillations in the combustion chamber is dependent on IMEP in previous cycles.

4. Conclusions

In summary, we would like to stress that the combustion process of natural gas has a complex dynamics.

Some insight into the process and its evolution with the changing equivalence ratio is revealed by several different statistical parameters. The large range of system responses on variable equivalence ratio (Figs. 2 and 3) makes it obvious that the main effect of fluctuation is coming from the dynamical process of combustion.

Furthermore, it is also worth to note that the presented multifractal approach has obvious advantages to quantify the combustion process using the measures of complexity and persistence. Such information could be useful for developing a more effective engine control strategy [43] improving capabilities of actual onboard real-time engine combustion control systems. It could also improve diagnostics for engine defects. In our multifractal calculations we used the software provided by physionet [36].

Acknowledgements

G. Litak has been partially supported by the 6th Framework Programme, Marie Curie Actions, Transfer of Knowledge, Grant No. MTKD-CT-2004-014058. B. F. Yao has been supported by the Scientific and Technological Innovation Fund for Excellent PhD Candidate of Beijing Jiaotong University.

[1] D. J. Patterson, SAE paper No. 660129 (1966).
[2] J. C. Kantor, Science **224**, 1233 (1984).
[3] Z. Hu, SAE paper No. 961197 (1996).
[4] R. M. Wagner, J. A. Drallmeier, and C. S. Daw, Int. J. Engine Research **1**, 301 (2001).
[5] C. S. Daw, C. E. A. Finney, and E. R. Tracy, Rev. of Scien. Instr. **74**, 915 (2003).
[6] M. Wendeker, G. Litak, J. Czarnigowski, and K. Szabelski, Int. J. Bifurcation and Chaos **14**, 1801 (2004).
[7] M. Wendeker, J. Czarnigowski, G. Litak, and K. Szabelski, Chaos, Solitons and Fractals **18**, 803 (2003).
[8] T. Kamiński, M. Wendeker, K. Urbanowicz, and G. Litak, Chaos **14**, 461 (2004).
[9] R. E. Winsor and D. J. Patterson, SAE paper No. 730086 (1973).
[10] J. W. Daily, Combustion Sci. Technol. **57**, 149 (1988).
[11] A. P. Foakes and D. G. Pollard, Combustion Sci. Technol. **90**, 281 (1993).
[12] L. Chew, R. Hoekstra, J. F. Nayfeh, and J. Navedo, SAE Paper No. 942486 (1994).
[13] C. Letellier, S. Meunier-Guttin-Cluzel, G. Gouesbet, F. Neveu, T. Duverger, and B. Cousyn, SAE Paper No. 971640 (1997).
[14] C. S. Daw, C. E. A. Finney, J. B. Green Jr., M. B. Kennel, J. F. Thomas, and F. T. Connolly, SAE paper No. 962086 (1996).
[15] C. S. Daw, M. B. Kennel, C. E. A. Finney, and F. T. Connolly, Phys. Rev. E **57**, 2811 (1998).
[16] J. A. Rocha-Martinez, T. D. Navarrete-Gonzalez, C. G. Pavia-Miller, R. Paez-Hernandez, and F. Angulo-Brown, Revista Mexicana de Fisica **48**, 228 (2002).
[17] G. Litak, R. Taccani, R. Radu, K. Urbanowicz, M. Wendeker, J. A. Hołyst, and A. Giadrossi, Chaos, Solitons and Fractals **23**, 1695 (2005).
[18] J. B. Green Jr., C. S. Daw, J. S. Armfield, C. E. A. Finney, R. M. Wagner, J. A. Drallmeier, M. B. Kennel, and P. Durbetaki, SAE Paper No. 1999-01-0221 (1999).
[19] A. K. Sen, G. Litak, R. Taccani, and R. Radu, Chaos, Solitons and Fractals **38**, 886 (2008).
[20] A. K. Sen, R. Longwic, G. Litak, and K. Górski, Mech. Syst. Signal Processing **22**, 362 (2008).
[21] N. Ozdor, M. Dulger, and E. Sher, SAE paper No. 940987 (1994).
[22] R. Radu and R. Taccani, SAE NA paper No. 2003-01-19 (2003).
[23] P. Boguś and J. Merkisz, Mech. Syst. Signal Processing **19**, 881 (2005).
[24] G. Litak, M. Wendeker, M. Krupa, and J. Czarnigowski, J. Vib. Control **11**, 371 (2005).
[25] G. Litak, T. Kamiński, R. Rusinek, J. Czarnigowski, and M. Wendeker, Chaos, Solitons and Fractals **35**, 578 (2008).
[26] G. Litak, T. Kamiński, J. Czarnigowski, D. Żukowski, and M. Wendeker, Meccanica **42**, 423 (2007).
[27] G. Litak, T. Kamiński, J. Czarnigowski, A. K. Sen, and M. Wendeker, Meccanica **4**, 1 (2009).
[28] G. X. Li and B.-F. Yao, Appl. Thermal Eng. **28**, 611 (2008).
[29] J. B. Heywood, Internal Combustion Engine Fundamentals, McGraw-Hill, New York 1988.
[30] Y. Goto and K. Narusawa, JSAE Rev. **17**, 251 (1996).
[31] A. E. Hassaneen and K. S. Varde, SAE paper No. 981384 (1998).
[32] P. Einewall and B. Johansson, SAE paper No. 2000-01-1941 (2000).
[33] K. S. Vardeet, SAE paper No. 2003-01-1935 (2003).
[34] W. Blumen, R. Banta, S. P. Burns, D. C. Fritts, R. Newsom, G. S. Poulos, and J. L. Sun, Dyn. Atmos. Oceans **34**, 189 (2001).
[35] J. F. Muzy, E. Bacry, and A. Arneodo, Phys. Rev. E **47**, 875 (1993).
[36] A. L. Goldberger, L. A. N. Amaral, L. Glass, J. M. Hausdorff, P. Ch. Ivanov, R. G. Mark, J. E. Mietus,

G. B. Moody, C.-K. Peng, and H. E. Stanley, Circulation **101**, E215 (2000), and the software provided on the webpage http://www.physionet.org/physiotools /multifractal/.

[37] H. Riedl, in: Long Range Dependence: Theory and Applications (Eds. P. Doukhan, G. Oppenheim, M. S. Taqqu), Birkhauser, Cambridge 2001, p. 625.

[38] L. Telesca and V. Lapenna, Tectonophysics **423**, 115 (2006).

[39] J. M. Nichols, S. T. Trickey, M. Seaver, and L. Moniz, J. Intelligent Mater. Syst. Struct. **18**, 51 (2007).

[40] G. Litak and J. T. Sawicki, in: Proc. of Euromech 498 Colloquium Kazimierz Dolny, Poland (Eds. J. Warminski, M. P. Cartmell, and J. Latalski, Lublin University of Technology 2008) 21st – 24th May 2008, pp. 210 – 213.

[41] A. K. Sen, G. Litak, T. Kaminski, and M. Wendeker, Chaos **18**, 033115 (2008).

[42] B. J. West, N. Scafetta, W. H. Cooke, and R. Balocchi, Ann. Biomed. Eng. **32**, 1077 (2004).

[43] K. Matsumoto, I. Tsuda, and Y. Hosoi, Z. Naturforsch. **62a**, 587 (2007).